Applied Clay Science 95 (2014) 182–190

Contents lists available at ScienceDirect

Applied Clay Science

journal homepage: www.elsevier.com/locate/clay

Research paper

Facile preparation of highly exfoliated and optically transparent polycarbonate (PC)/clay mineral nanocomposites using phosphonium modified organoclay mineral

Supratim Suin, Nilesh K. Shrivastava, Sandip Maiti, B.B. Khatua *

Materials Science Centre, Indian Institute of Technology, Kharagpur 721302, India

ARTICLE INFO

Article history:
Received 16 May 2013
Received in revised form 17 February 2014
Accepted 5 April 2014
Available online 30 April 2014

Keywords:
PTPP-Mt
Optical transparency
PC
Thermomechanical property

ABSTRACT

Here, we focus on the morphology, mechanical and optical properties of the polycarbonate (PC) in the PC/clay mineral nanocomposites prepared through both the melt and solution blending technique at two different loadings (0.5 phr and 1 phr) of propyl triphenyl phosphonium modified montmorillonite (PTPP-Mt). The modified organo-Mt was prepared by ion exchange reaction and verified through FTIR spectroscopy, EDS study and XRD analysis. The outstanding thermal stability of the PTPP-Mt at the processing temperature of PC (280 °C) made it a suitable candidate for the preparation of optically transparent PC/Mt nanocomposites. The XRD analysis over the PC/PTPP-Mt nanocomposites revealed the destruction of ordered geometry of the clay mineral, whereas, the presence of some localised zones of Mt was evident from transmission electron microscopic (TEM) analysis. Thermal analysis indicated an increase in glass transition temperature (T_g) and thermal stability of PC in the nanocomposites. The strength and modulus of the nanocomposites were increased with increase in Mt loadings. An increase in storage modulus in the nanocomposites was evident from the thermomechanical studies. Finally, the optical transparency of PC was retained without generation of any colour in the PC/PTPP-Mt nanocomposites.

1. Introduction

Polycarbonate (PC) is a well-known optically transparent, amorphous, engineering thermoplastic possessing excellent thermal stability, impact property and heat distortion temperature (HDT). But, it suffers from very poor chemical resistance (LeGrand and Bendler, 2000). Layered silicates of nanometre thickness are reported to increase chemical resistivity with concomitant increase in mechanical and thermal properties (Friessell and Bikales, 1967). If it can be done without affecting much the optical properties many practical and commercial applications can be resolved.

Montmorillonite (Mt), a smectite layered-silicate, consists of stacks of 1 nm thick aluminosilicate layers regularly spaced. Each layer contains a central sheet of octahedral-Al sandwiched between two tetrahedral silicate sheets. Isomorphic substitutions of trivalent aluminum by bivalent magnesium in the octahedral sheet result negative charges, which are being compensated by the alkaline earth- or hydrated alkali metal cations present in between two aluminosilicate layers (Bailey, 1980, 1984). The van der Waals and electrostatic forces holding the layers together are relatively weak in the Mt. The ease of swelling of high aspect ratio layers in water makes them suitable substrates for surface ion exchange with alkyl ammonium, phosphonium, imidazolium etc ions. These modifiers modify the surface of the clay mineral layers to make them compatible with organic polymer matrices to achieve good interaction between them (Lagaly and Beneke, 1991; Theng, 1974).

Polymer/layered silicate nanocomposites have attracted various research groups, because of its unique sets of properties depending on the range of interaction between the polymer and the nano-dispersed clay silicate layers (Sinha Ray and Okamoto, 2003). Naturally occurring clay mineral is hydrophilic in nature, whereas, major polymers are organophilic in nature. Thus, for better dispersion and interaction of the hydrophilic clay mineral with the organophilic polymers, clay mineral is required to be modified with quaternary ammonium (Carrion et al., 2008; Chow and Neoh, 2010; Guduri and Luyt, 2008; Hsieh et al., 2004; Huang et al., 2000; Lee and Han, 2003; Mitsunaga et al., 2003; Nevalainen et al., 2009; Wu et al., 2007; Yoon et al., 2003a, 2003b), phosphonium (Avalos et al., 2009; Cai et al., 2010; Calderon et al., 2008; Gilman et al., 2002; Patro et al., 2009; Rama and Swaminathan, 2010; Saitoh et al., 2011; Wang et al., 2012; Xiang et al., 2010; Xie et al., 2002) imidazolium (Cui et al., 2009; Gilman et al., 2002; Rama and Swaminathan, 2010) ions etc. These bulky ions not only help to increase the compatibility between polymer and clay mineral, but also favour the intercalation of polymer chains into the interlayer spaces of the clay.

* Corresponding author at: Materials Science Centre, Indian Institute of Technology, Kharagpur-721302, India. Tel.: +91 3222 283978.
E-mail address: khatuabb@matsc.iitkgp.ernet.in (B.B. Khatua).

http://dx.doi.org/10.1016/j.clay.2014.04.009
0169-1317/

Depending on the method of composites preparation and state of dispersion of clay minerals in the matrix polymer, three different microstructures may appear in the polymer/clay mineral nanocomposites. When the polymer fails to intercalate between the silicate sheets, a phase separated composite is obtained. In intercalated structure, a single (or more) polymer chain intercalates between the silicate layers, resulting in a well-ordered multilayer morphology built up with alternating polymeric and inorganic layers. When the ordered structure of the clay minerals gets destroyed and the individual silicate layers get completely and uniformly dispersed in the continuous polymer matrix, an exfoliated or delaminated structure is obtained. Polymer/clay mineral nanocomposites can be prepared by three conventional methods, such as, (a) *in-situ* polymerization of monomers in presence of clay mineral (Jash and Wilkie, 2005; Sain and Khatua, 2011; Su and Wilkie, 2003; Xie et al., 2003) (b) solution blending (Gao et al., 2001; Yeh et al., 2004) and (c) melt blending (Carrion et al., 2008; Chow and Neoh, 2010; Guduri and Luyt, 2008; Hsieh et al., 2004; Huang et al., 2000; Lee and Han, 2003; Mitsunaga et al., 2003; Nevalainen et al., 2009; Wu et al., 2007; Yoon et al., 2003a, 2003b). Among these three manufacturing methods, melt blending is most demanding because of its industrial acceptance.

A number of research articles have been reported in the literature concerning the properties of PC/clay mineral nanocomposites using different modified clay minerals. Huang et al., 2000 prepared successfully intercalated-exfoliated PC/clay mineral nanocomposites via ring opening polymerization using lower molecular weight cyclic carbonate oligomers and ditallow dimethyl quaternary ammonium substituted montmorillonite. Lee and Han, 2003 studied the effect of H-bonding on the morphology and properties of PC/Mt nanocomposites. Their study revealed that, the H-bonding between the carbonyl group of PC and the active functional group presents in the modifier was responsible for the exfoliation of the clay mineral in the twin-screw extruded PC/clay mineral nanocomposites. Yoon et al., 2003a, 2003b made a detailed study over various molecular weight PC and different ammonium modified clay minerals to investigate the effect of molecular weight of PC and organoclay mineral structure on the morphology and properties of PC/clay mineral nanocomposites. They reported that, the high shear force generated during the melt processing of high molecular weight PC resulted in high degree of dispersion of clay mineral layers into the PC matrix. A consequent paper revealed that, the reduction of molecular weight and occurrence of colour in the melt blended PC/clay mineral nanocomposites was dependent on residence time in the extruder, chemical structure of the modifier, and the iron content of the clay mineral (Yoon et al., 2003a, 2003b). Guduri and Luyt, 2008 studied the effect of PP-g-MA on the morphology and mechanical properties of melt intercalated PC/clay mineral nanocomposites. The morphological study revealed that, the extent of exfoliation of the clay minerals was increased with increasing amount of PP-g-MA in the nanocomposites. Hsieh et al., 2004 concentrated on the mechanical and rheological properties of melt-intercalated PC/clay mineral nanocomposites. They reported that, during melt blending, the degradation of PC matrix was related to the loading of clay mineral in the nanocomposites, which in turn decreased the T_g and molecular weight of the PC in the nanocomposites. Mitsunaga et al., 2003 studied the effect of a compatibilizer in the melt intercalated PC/clay mineral nanocomposites. Their study revealed that, the morphology of the clay mineral in the nanocomposites and the degradation of the matrix phase were dependent on the surfactants present in the modified clay mineral and the compatibilizer used. Wu et al., 2007 studied the effect of epoxy resin on the rheological properties of melt-intercalated PC/clay mineral nanocomposites. They reported that, the addition of epoxy at lower amount favoured the dispersion of clay mineral layers, whereas, the higher loading of epoxy played the role of a plasticizer that resulted in severe degradation of the PC matrix. Rama and Swaminathan, 2010 studied the morphology and optical properties of the PC/Mt nanocomposites prepared through *in-situ* melt polycondensation using phosphonium and imidazolium modified organoclay mineral. A highly exfoliated morphology was developed with generation of dark brown colour in the nanocomposites.

The literature discusses mainly the morphology and mechanical properties of the PC/clay mineral nanocomposites in presence of different modified clay minerals without giving much attention on the optical properties and colour issues. Moreover, most of the works deal with the ammonium modified organoclay minerals. Conventional ammonium modified organoclay minerals can hardly sustain at the processing temperature of PC (≈280 °C) and thus degrades during the preparation of PC/clay mineral nanocomposites. This sort of degradation of the modified clay minerals generates reactive radicals, which transform PC chains into coloured quinoid form and thus the optical transparency of PC gets destroyed (Feng et al., 2012; Xie et al., 2001). This work deals with the preparation and properties of PC/Mt nanocomposites through conventional melt and solution blending process, using phosphonium modified clay mineral. The effect of the thermally stable organoclay mineral on the morphology, mechanical and optical properties has been described in the manuscript in detail.

2. Experimental

2.1. Materials used

The bisphenol-A polycarbonate (PC), used as the base matrix, was of commercial grade (Lexan 143, MFI ≈10.5 g/10 min at 300 °C and 1.2 kg load), supplied by SABIC Innovative Plastics. The unmodified naturally occurring clay mineral (sodium montmorillonite, Na-Mt) was procured from Southern Clay Products, Inc., USA. The cation exchange capacity (CEC) of the supplied Na-Mt is 92 mequiv/100 g of clay mineral. The organic modifier, propyl triphenylphosphonium bromide (PTPP-Br) was purchased from Sigma-Aldrich. Methanol and dichloromethane were supplied by Merck, Germany.

2.2. Modification of the Mt

The modification of the pristine clay mineral (Na-Mt) was done through the ion exchange reaction following the method described in our previous paper (Suin and Khatua, 2012) using PTPP-Br in water medium. In a beaker 2.5 g of Na-Mt was dispersed in 250 ml de-ionized water by ultrasonication (OSCAR Model PR-250; ultrasonic power 250 W, frequency 25 kHz, probe tip diameter 6 mm) at room temperature for 1 h to destroy the ordered structure of the clay mineral in the water medium. The clay mineral/water suspension was then transferred in a 2 L three neck round bottom flask (R. B. flask) containing 500 ml water and stirred for 45 min, using an overhead stirrer. The reactor temperature was maintained at 80 °C throughout the reaction. Based on the CEC value (92 meqiv/100 g) of the Na-Mt, calculated amount (~1 g) of the quaternary phosphonium salt (PTPP-Br) was dissolved in 50 ml de-ionized water. The PTPP-Br solution was then added drop wise over a period of 10 min to the dispersion of Na-Mt in the reaction flask under stirring condition. The addition of the PTPP-Br solution was followed by the settling down of the clay mineral agglomerates. The introduction of the organic moiety into the interlayer space of the clay minerals was responsible for the generation of hydrophobicity in the clay mineral, which in turn helped the settling down of the clay minerals. The reaction was continued for another 2 h for the completion of the ion exchange reaction. The resulting clay mineral agglomerates were filtered by vacuum filtration and then washed by hot water to remove the undesired impurity (NaBr and unexchanged propyltriphenylphosphonium bromide). The washing was continued till the filtrate was free from bromide ions, as examined by a dilute $AgNO_3$ solution. The final washing was carried out by using 250 ml methanol to eliminate the excess propyltriphenylphosphonium ions present in the interlayer spaces of the clay mineral. The moist clay mineral, obtained after final filtration, was first air-dried and then under

vacuum at 80 °C for 12 h. The oven-dried clay mineral aggregates were then grinded to fine powder by mortar and pastel.

2.3. Preparation of the PC/PTPP-Mt Nanocomposites

Here we have considered two blending techniques (melt and solution blending) for the preparation of PC/PTPP-Mt nanocomposites at two different loadings of PTPP-Mt (0.5 and 1 phr), as described below:

2.3.1. Melt mixing

Prior to the melt mixing, desired amount of PC and the PTPP-Mt were dried in a vacuum oven at 80 °C for 6 h to avoid any moisture induced thermal degradation of the components during blending. Melt-blending of the PC with PTPP-Mt was done in an internal mixer (Brabender Plasticorder with chamber capacity of 20 cc; S.C. Dey & Co., Kolkata, India) at 280 °C, 60 rpm for 15 min. Finally, the melt-mixed PC/PTPP-Mt nanocomposites lumps were injection molded at 280 °C into desired shapes for further characterizations.

2.3.2. Solution casting

In a 250 ml beaker, 20 g PC was allowed to dissolve in 100 ml of dichloromethane (DCM) at room temperature. In another beaker, calculated amount (0.1 and 0.2 g) of the PTPP-Mt was well dispersed in 60 ml DCM by using ultrasonic probe sonicator at room temperature. After 30 min of sonication, the PC/DCM solution was gradually added into the PTPP-Mt/DCM suspension for a period of 5 min under constant sonication. The sonication of PC/PTPP-Mt solution mixture was allowed for another 30 min. Finally, the mixture was stirred for 15 min at 60 rpm with a magnetic stirrer at room temperature to evaporate the solvent and make the solution more viscous. The resulting mixture was transferred in a Petri-dish. The final composite flakes were obtained after the evaporation of the DCM in air. The resulting composite flakes were first dried in air and the final solution blended nanocomposites material was obtained after complete removal of the solvent in a vacuum oven.

3. Characterizations

3.1. Fourier transform infrared (FTIR) spectroscopy

The FTIR spectroscopic analysis of the Mt before and after modification was carried out on a NEXUS 870 FTIR (Thermo Nicolet) instrument. The pellets were obtained after grinding the clay minerals with spectroscopic grade KBr and introducing into the pelletizer. FTIR spectra of the clay minerals were recorded using the pellets in the range of 4000–400 cm^{-1}.

3.2. X-ray diffraction Analysis

The d_{001} distance of the unmodified Na-Mt, the phosphonium modified PTPP-Mt and their nanocomposites with PC was measured by using a wide angle X-ray diffractometer, (WAXD, Rigaku, Ultima-III, Japan) with nickel-filtered CuK_α line ($\lambda = 0.15404$ nm) operated at an accelerating voltage of 40 kV and 40 mA, at a scanning rate of 0.5 °/min. The distance between the sample and detector was 400 mm. The d_{001} distance of the ordered structure of the layered silicates was determined by using the Bragg's law ($n\lambda = 2d\sin\theta$), where, d represents the distance between the d_{001} planes in the layered silicate, λ is the wave length of the incident wave and θ is the angle between the incident wave and the scattering planes, and n is an integer.

3.3. TEM analysis

The morphological analysis of the nanocomposites samples were also done by direct visualisation of the clay mineral layers in the PC matrix by transmission electron microscopy (HRTEM: JEM-2100, JEOL, Japan) operating at an accelerating voltage of 100 kV. The PC/Mt nanocomposites samples were ultramicrotomed by incorporating a diamond cutter with a thickness of 100 nm. Since the clay mineral layers possess much higher electron density than the polymer (PC), no staining was required and the clay mineral layers appeared dark in the TEM images. Energy dispersive X-ray spectroscopy (EDS) analysis of the Na-Mt and the PTPP-Mt were carried out by casting the dispersed samples on Cu grids.

3.4. Differential scanning calorimetry (DSC)

The T_g of the neat PC and the PC/PTPP-Mt nanocomposites was determined with differential scanning calorimetry (DSC-200 PC, NETZSCH). In DSC experiment, 10–12 mg of sample was first heated (in nitrogen atmosphere) from room temperature to 330 °C and held at 330 °C for 5 min to remove the moisture and previous thermal history. Then the sample was allowed to cool to room temperature and reheated to 330 °C. The T_g of the samples was determined from the second heating curve. The heating and the cooling rate was 10 °C/min throughout the test procedure.

3.5. Thermogravimetric analysis (TGA)

The thermal stability of the neat PC and its nanocomposites with PTPP-Mt was studied employing a TGA V 50 IA Dupont 2100 thermo gravimetric analyzer in nitrogen atmosphere in the temperature range of 30–800 °C, with a heating rate of 10 °C/min. The isothermal TGA scan for the PTPP-Mt, at the processing temperature of PC (280 °C) was carried out to examine the stability of the modified Mt at the processing temperature of the PC.

3.6. Tensile properties

The tensile properties of the pure PC and the PC/PTPP-Mt nanocomposites was carried out on dumb-bell shaped injection molded samples using a Tinius Olsen H 50 KS (universal testing machine) at room temperature with a gauge length of 23 mm, width 4.8 mm, thickness 2 mm and crosshead speed of 5 mm/min. Here, the reported values are the average of the results for tests run on at least five specimens.

3.7. Dynamic mechanical analysis (DMA)

The thermo-mechanical properties (storage modulus) of the pure PC and the PC/PTPP-Mt nanocomposites were measured by a dynamic mechanical analyzer (DMA 2980 model, TA Instruments Inc., USA), using injection molded impact bar samples. The dynamic temperature spectra of the PC, as well as the PC/PTPP-Mt nanocomposites were obtained in tension film mode at a constant vibration frequency of 1 Hz, temperature range of 40–170 °C at a heating rate of 5 °C/min in nitrogen atmosphere. The dimension of the specimen was $32 \times 12.5 \times 3.5$ mm^3.

3.8. UV-vis spectroscopy

The UV-vis spectroscopic analysis was performed to examine the optical transparency of the pure PC and melt and solution blended PC/clay nanocomposites using solid films. The melt compounded films were obtained after compression molding at a constant pressure. To prepare the solution casted films, 0.5 g of pure PC and the solution casted nanocomposites samples were dissolved separately in 15 ml dichloromethane (DCM). The DCM solutions were poured separately over different Petri-dishes having uniform surface. The evaporation of DCM solvent at room temperature yielded the solid films. For comparison, the percent transmittance was measured as a function of wavelength by using Perkin Elmer, Lambda 750 spectrophotometer.

4. Results and discussion

4.1. Analysis of the PTPP-Mt

4.1.1. FTIR study

The FTIR spectral responses of the Mt before and after modification are depicted in Fig. 1. As can be seen, the unmodified Mt (Fig. 1a) gave rise to characteristic bands at 3620, 1040, 516 and 460 cm^{-1} consistent with the different modes of bond vibrations of the alluminosilicate moiety present in the basic Mt part. The 'O-H' stretching vibration revealed the highly intense peak at 3620 cm^{-1}. The bands at 1040 and 460 cm^{-1} are corresponding to the 'Si-O' stretching and 'Si-O-Si' bending vibrations, respectively. The band at 516 cm^{-1} is related to the 'Al-O' stretching vibration. The broad peak centred at ~3400 cm^{-1} could be associated with the vibrations of the water molecules present in the Mt. The appearance of bands at 1430 and 1115 cm^{-1} are related to the in plane and out of plane bending vibration of the PPh_3, respectively (Fig. 1b), presented in the PTPP-Mt. The peaks at 2860 and 2920 cm^{-1} could be related to C-H symmetric and asymmetric stretching of methylene ($-CH_2-$) group present in the modifier. Thus, the incorporation of propyl triphenyl phosphonium moiety (phosphonium modifier) in the interlayer space of Na-Mt during ion exchange reaction was evident from the IR spectroscopic analysis.

4.1.2. EDS analysis of the PTPP-Mt

The elemental analysis (EDS study) of the pure Na-Mt and the modified PTPP-Mt was carried out to verify the elements present in the corresponding clay minerals. Fig. 2 shows the EDS spectra of the Mt before (Fig. 2a) and after (Fig. 2b) ion exchange reaction. As can be observed, Na-Mt consists of oxygen, aluminium and silicon as major elements with traces amount of sodium, magnesium and iron. The sodium peak disappeared with the appearance of carbon, phosphorus (along with the oxygen, aluminium, silicon, magnesium and iron) in the EDS spectra of the modified Mt. The EDS spectra are indicative to the replacement of the sodium ions with quaternary phosphonium ions in the interlayer spaces of the unmodified Mt during ion exchange reaction.

4.1.3. XRD analysis of the PTPP-Mt

Fig. 3 represents the XRD patterns of the unmodified Na-Mt and the phosphonium modified PTPP-Mt. The characteristic peak of Na-Mt was appeared at $2\theta \approx 7.12$, corresponding to the d_{001} distance of ≈1.24 nm. The corresponding peak for the PTPP-Mt was shifted to a lower region ($2\theta \approx 4.9$), indicating the increase in d_{001}-spacing (≈1.8 nm) in the PTPP modified Mt. This XRD results for the unmodified and the modified clay minerals unambiguously led us to assume replacement of the smaller Na^+ ions by bulky quaternary phosphonium ions in the interlayer space of the Na-Mt that resulted the phenomenal increase in the d_{001} distance of the Mt layers after ion-exchange reaction.

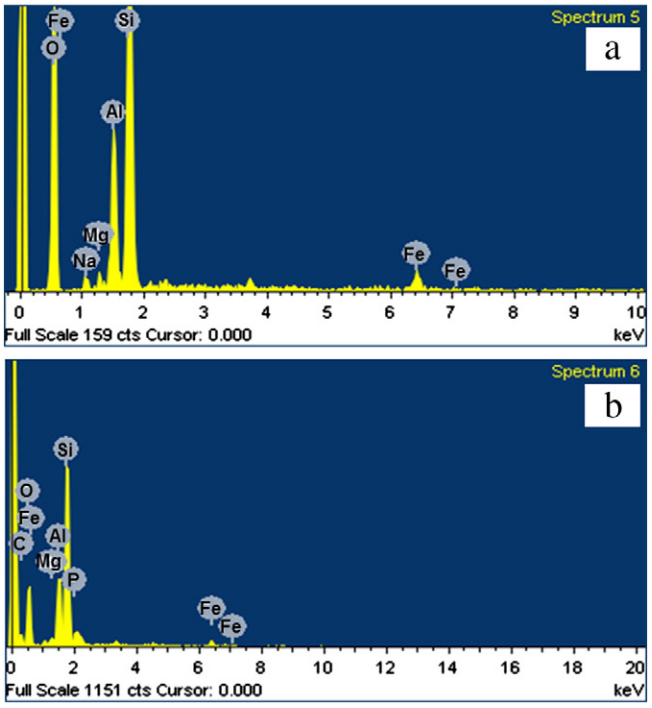

Fig. 2. EDS spectra of (a) Na-Mt, (b) PTPP-Mt.

4.1.4. Thermal stability of the modified Mt

Isothermal TGA scan for the modified Mt was carried out at the processing temperature of PC (280 °C) to investigate the stability of the PTPP-Mt at the said temperature. The PTPP-Mt was allowed to stand for 20 min in isothermal condition in oxygen atmosphere. A residual mass of ≈98.76% was evident after 20 min at 280 °C, suggesting ~1.24% degradation of the clay mineral during this period. This TGA results also indicated the high potentiality of the PTPP-Mt in the preparation of PC/Mt nanocomposites with retained optical transparency of PC.

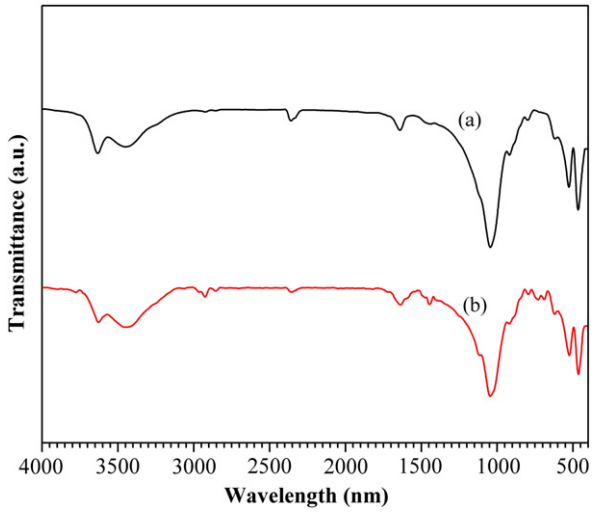

Fig. 1. FTIR spectra of (a) Na-Mt and (b) PTPP-Mt.

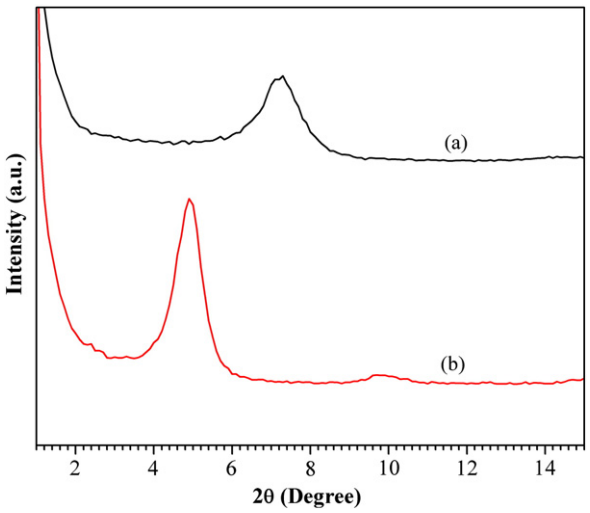

Fig. 3. XRD patterns of the (a) Na-Mt and (b) PTPP-Mt.

4.2. Analysis of the PC/PTPP-Mt nanocomposites

4.2.1. XRD analysis

The XRD patterns of the PTPP-Mt and its nanocomposites with PC, prepared through the melt and solution blending at two different loadings (0.5 phr and 1 phr) of the clay mineral are depicted in Fig. 4. As can be seen, irrespective of the method of nanocomposites preparation and loading of Mt, the characteristic peak (Fig. 4a) for the ordered structure of PTPP-Mt (at $2\theta \approx 4.8^{\circ}$) was disappeared in the nanocomposites. A well exfoliated morphology of Mt in the PC/PTPP-Mt nanocomposites was evident from the XRD patterns. The high level of dispersion of the clay mineral layers in the melt blended nanocomposites can be explained in terms of the high shear force generated from the melt mixing of high molecular weight PC. Again, in solution blending process the clay mineral layers were first forced to disperse randomly in DCM solvent under high energy ultrasonication. Then, the viscous PC/DCM solution was added to the Mt/DCM solution. The high viscosity of the resulting nanocomposites solution prevented the re-aggregation of the clay mineral layers and the composites appeared as highly exfoliated. However, the inadequacy in the amount of the clay minerals in the nanocomposites to result in the characteristic peak of Mt cannot be discarded. Thus, the TEM analysis was very much significant for the concluding remarks regarding the dispersion of the clay mineral layers in the PC matrix.

4.2.2. TEM analysis

The TEM analysis of the PC/PTPP-Mt nanocomposites samples were carried out to verify the state of dispersion of the clay mineral layers into the bulk. Fig. 5 shows the microstructural images of the nanocomposites samples, obtained from TEM analysis. From Fig. 5a, it is obvious that the ordered geometry of the Mt got destroyed and the clay mineral layers got highly distributed and dispersed into the matrix PC at lower loading of Mt (0.5 phr), irrespective of the methods of nanocomposites preparation. The highly delaminated morphology of the Mt layers can also be observed at the high magnification image (Fig. 5b). To explain the phenomemon we assume that the intercalation of the surfactant molecules inside the interlayer spaces increased the d_{001} distance in the PTPP-Mt (as observed XRD analysis of the Mt). The expansion of the interlayer space helped in the incorporation of the PC chains into the galleries with successive delamination of the clay mineral layers under high shear force (kinetically favourable) during melt-mixing. The nanocomposites at higher loading (1 phr) appears as a materials possessing some aggregated layers of Mt, while most of the clay mineral layers got randomly dispersed into the matrix PC (Fig. 5c). A more critical evaluation of the sample by higher magnification image revealed the absence of any aggregated zones (Fig. 5d), rather the presence of some of the clay mineral layers in a very close proximity which appeared as aggregated in the low magnification image.

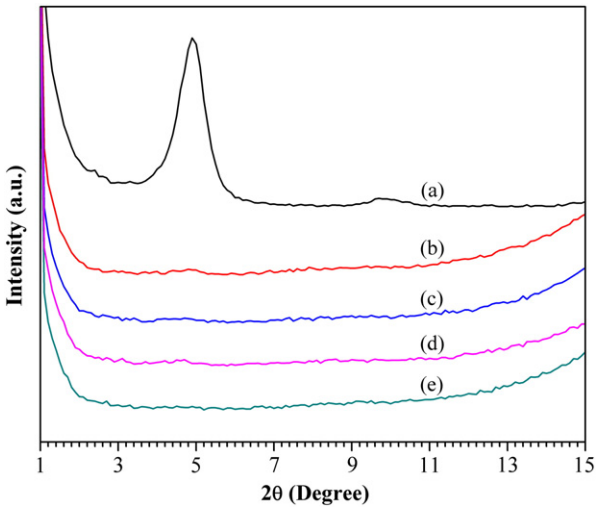

Fig. 4. XRD plots of (a) PTPP-Mt; melt-blended PC/PTPP-Mt nanocomposites with: (b) 0.5phr PTPP-Mt, (c) 1phr PTPP-Mt; solution-blended PC/PTPP-Mt nanocomposites with: (d) 0.5 phr PTPP-Mt, (e) 1phr PTPP-Mt.

It was interesting to find that, the prepared nanocomposites possessed organoclay mineral devoid of any long chains in the modifier, as previously reported by most of the groups to prepare polymer/clay mineral nanocomposites. Most of the commercially available nanoclay minerals (Cloasite 30B, SCPX 2004 etc.) possessed a long aliphatic chain of at least 12 carbons. Here, the incorporated organic moiety consists of three phenyl group along with one propyl group. The steric hindrance between the aromatic rings favoured the expansion of interlayer space and the d_{001} value was found to be 1.8 nm, which is quite similar to the d_{001} value of SCPX 2004 (1.8 nm), cloisite 30B (1.86 nm) etc. So, the interlayer space of ~ 1.8 nm can be considered sufficient for the easy intercalation of the polymer chains. In this work, we considered PTPP modified Mt (possessing shorter chain) as the modified clay mineral to minimize the degradation of organoclay mineral during melt-mixing and thus the optical transparency of the PC was retained in the nanocomposites. Moreover, the easy intercalation of the PC chains in side the clay mineral layers followed by the shear force during melt blending (or, the ultrasonic vibration during solution blending) favoured the orientation of the Mt layers in a highly dispersed form in the PC/PTPP-Mt nanocomposites.

4.2.3. DSC study

DSC analysis was carried out to compare the T_g of the PC/PTPP-Mt nanocomposites with that of pure PC. The effect PTPP-Mt on the T_g of PC/PTPP-Mt nanocomposites at two different PTPP-Mt loadings (0.5 phr and 1 phr), prepared through both the blending techniques are depicted in Fig. 6. The intercalation of the polymer chains into the interlayer spaces leads to the confinement of the polymer chains and thus results in an increase in T_g in the nanocomposites (Lu and Nutt, 2003; Yu et al., 2003). However, irrespective of the methods of nanocomposites preparation, a nominal change in T_g ($\approx$150 °C) was evident in the 0.5 phr PTPP-Mt loaded PC/PTPP-Mt nanocomposites. The high level of dispersion of clay mineral layers in the matrix PC was unable to affect the segmental motion of the PC chains, which might be an effective reason for the slight increment in T_g. Moreover, a marginal (2–3 °C) increase in T_g was occurred in case of higher loading (1 phr) of PTPP-Mt in the nanocomposites. This sort of increase in T_g with increase in PTPP-Mt loading can be explained in terms of the increase in interacting area between the PC and the clay mineral layers which may result some restriction in the bond segmental motion of the PC chains in the nanocomposites.

4.2.4. TGA analysis

The stability of the organic surfactant ions present in the interlayer spaces as well as the amount of the inorganic content generally affects the thermal stability of the polymer/Mt nanocomposites. Fig. 7 depicts the dynamic TGA scans of the neat PC and its nanocomposites with different proportion of PTPP-Mt, prepared through both the blending techniques. The detailed thermogravimetric studies has been done in terms of onset degradation temperature (T_0, corresponding to 5% wt loss) and T_{50} (temperature corresponding to 50% wt loss). As observed, irrespective of the methods of nanocomposites preparation, the T_0 and T_{50} were increased with increase in the Mt loading in the PC/PTPP-Mt nanocomposites. For instance, the incorporation of 0.5 phr Mt, increased the T_0 of neat PC (449 °C) to $\approx$467 °C and $\approx$465 °C for melt blended and solution blended PC/PTPP-Mt nanocomposites, respectively. However, the clay mineral at higher loadings (1 phr) increased the T_0 by $\approx$15 °C compared to that of neat PC in the melt and solution blended nanocomposites. The T_{50} of PC/PTPP-Mt nanocomposites prepared through both the blending techniques followed the similar trend. The T_{50} of the virgin PC (511 °C) was appeared at $\approx$516 °C and $\approx$521 °C for the 0.5 phr and 1 phr PTPP-Mt loaded PC/PTPP-Mt nanocomposites, respectively. From the TGA

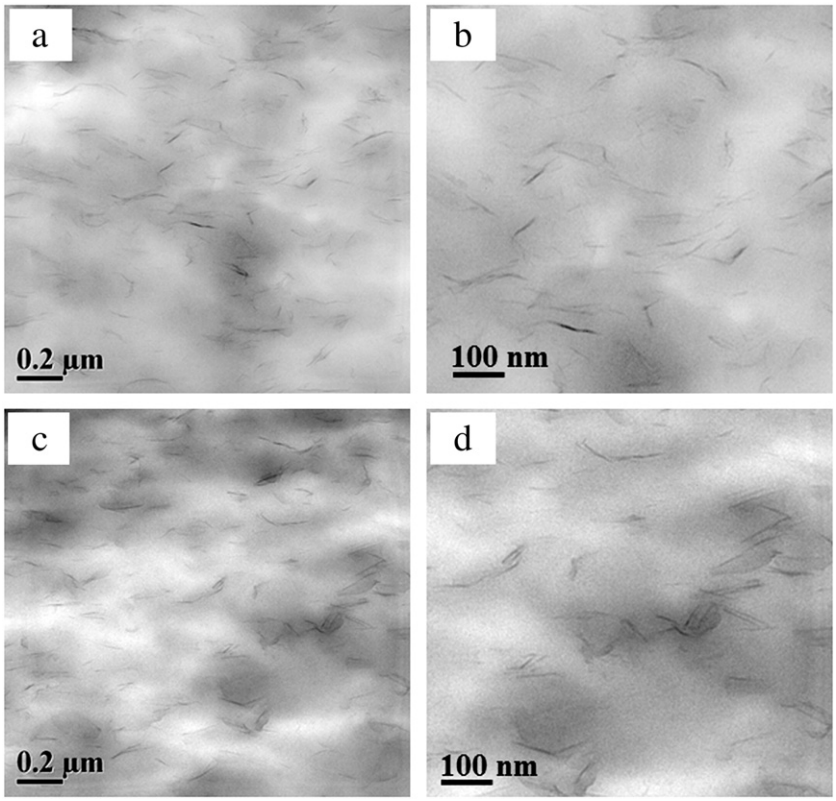

Fig. 5. HRTEM images of (a, b) 0.5 phr and (c, d) 1phr PTPP-Mt loaded PC/PTPP-Mt nanocomposites at two different magnifications: (a, c) low magnification, (b, d) high magnification. In all the cases the nanocomposites are melt blended.

thermogramms it can be concluded that, the incorporation of the PTPP-Mt increased the thermal stability of the matrix PC in the PC/PTPP-Mt nanocomposites. The increase in thermal stability could be associated with the shielding effect of the clay mineral layers along with the inherent flame retardant property of the phosphonium modified organoclay mineral (Zheng and Wilkie, 2003). Moreover, the inorganic content present in the nanocomposites restricts the intimate contact of the heat with the polymer, and thus reduces the diffusion of heat into the bulk of the nanocomposites (Suin et al., 2013). It was very interesting to observe that the TGA plots followed almost similar trends in both

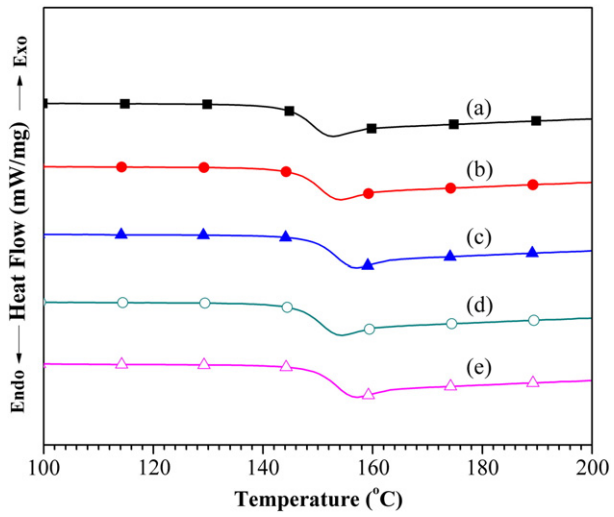

Fig. 6. DSC thermograms of (a) Neat PC, melt-blended PC/PTPP-Mt nanocomposites with: (b) 0.5phr PTPP-Mt, (c) 1phr PTPP-Mt; solution-blended PC/PTPP-Mt nanocomposites with: (d) 0.5phr PTPP-Mt, 0 1phr PTPP-Mt.

the melt and solution blended nanocomposites, suggesting indirectly the presence of almost similar morphology of PTPP-Mt, as discussed in XRD and TEM analysis.

4.2.5. Mechanical properties

The effect of the Mt loadings and processing technique on the mechanical properties (tensile strength, Young modulus and elongation at break) of PC/PTPP-Mt nanocomposites are depicted in Table 1. As can be seen, irrespective of the methods of nanocomposites preparation, the tensile strength and Young modulus of the PC was increased in the PC/PTPP-Mt nanocomposites and was dependent on the loading of the PTPP-Mt. The huge interacting area between the PC and the surface of stiff clay mineral layers of high aspect ratio in a well exfoliated morphology of PTPP-Mt in the nanocomposites is the effective reason for the phenomenal increase in the strength and modulus (Lu and Mai, 2005). However, the elongation at break was decreased with the increase in PTPP-Mt loading in both the melt and solution processed nanocomposites. This sort of increase in percent elongation with increase in PTPP-Mt loading can be explained in terms of the increase in stress concentration with the incorporation of organoclay mineral in the PC matrix, resulting in an enhanced brittleness in the nanocomposites (Mishra et al., 2005).

Fig. 8 represents the temperature dependence storage modulus of the pure PC and its nanocomposites with PTPP-Mt at two different loadings of PTPP-Mt. From the figure it is obvious that, the storage modulus of the nanocomposites, prepared through both the melt and solution blending, was improved in both the glassy and rubbery regions. The increase in storage modulus might be associated with the reinforcing effect imparted by the high aspect ratio clay mineral layers, favouring a higher degree of stress transfer at the interface between the PC and clay mineral (Hasegawa et al., 1999). Moreover, with increase in PTPP-Mt loadings the surface area of clay mineral layers increases in case of highly exfoliated morphology. As the storage modulus of the nanocomposites is directly related to the interacting area between the

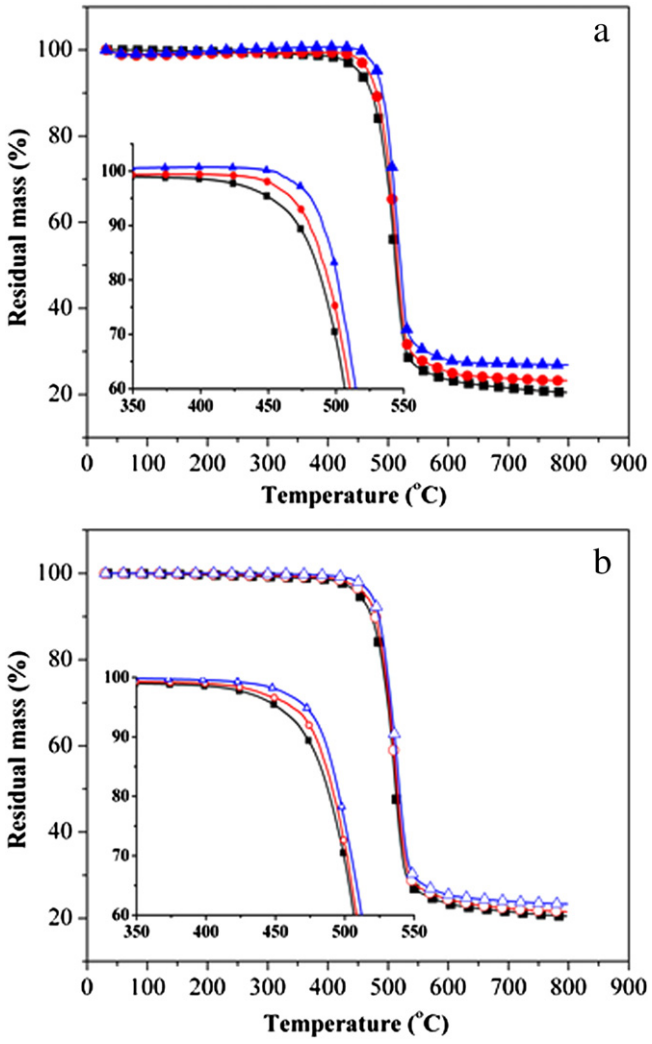

Fig. 7. TGA thermograms of (■) neat PC; and its (a) melt blended (●,▲), (b) solution blended (○,△) nanocomposites with 0.5 phr PTPP-Mt (●,○), 1 phr PTPP-Mt (▲,△).

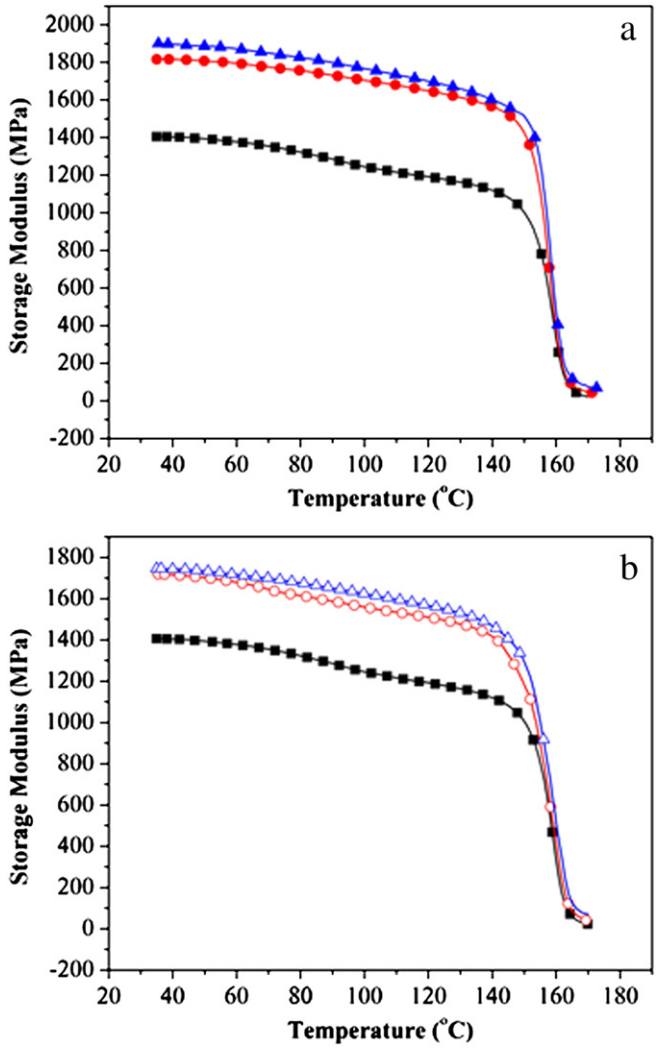

Fig. 8. Storage modulus of neat PC (■); and its (a) melt blended (●,▲), (b) solution blended (○,△) nanocomposites with 0.5 phr PTPP-Mt (●,○), 1 phr PTPP-Mt (▲,△).

polymer and Mt, the storage modulus should increase with increase in PTPP-Mt in case of exfoliated PC/PTPP-Mt nanocomposites.

The variation of damping factor (tan δ) with temperature for both the melt and solution blended nanocomposites is plotted in Fig. 9. The T_g value can be predicted from the peak value of tan δ plot. The tan δ plot predicted a T_g value of 152 °C for the pure PC, which was increased to ≈154 °C at 0.5 phr PTPP-Mt in both the melt and solution blended PC/PTPP-Mt nanocomposites. As the clay mineral layers got extensively dispersed in the PC matrix, the segmental motion of the PC chains will be less affected, as compared to that in an intercalated nanocomposites. The nanocomposites at higher loading of PTPP-Mt possessed a T_g value of ≈157 °C, owing almost the similar trend obtained from DSC analysis.

The variation in T_g, thermal stability and mechanical properties, as reported earlier by various groups in case of polymer/clay mineral nanocomposites system is summarized in Table 2. From the data, it can easily be concluded that, the thermal and mechanical properties of polymer clay nanocomposites depends not only on the polymer and clay mineral itself, rather depend on several other factors, such as, method of composite preparation, surfactant present in the clay and morphology of the clay in the final nanocomposites.

4.2.6. Optical properties

The comparison of optical transparency of the pure PC and the PC/PTPP-Mt nanocomposites films were done by UV-vis spectroscopic study. For the said purpose, the percent transmittance of the melt and solution blended nanocomposites films (thickness 40–50 μm) were compared with the pure PC film of similar thickness at varying wavelength (300–700 nm) and plotted in Fig. 10. A very nominal change

Table 1
Mechanical properties (tensile strength, Young modulus and elongation at break) of Pure PC and PC/PTPP-MMT nanocomposites.

Sample	Tensile strength (MPa)	Young modulus (MPa)	Elongation at break (%)
Pure PC	46.3 ± 1.2	1098 ± 36	8.46 ± 0.56
PC/0.5 phr PTPP-MMT (melt)	57.2 ± 2.1	1360 ± 55	6.92 ± 0.42
PC/1 phr PTPP-MMT (melt)	60.8 ± 2.5	1433 ± 74	5.9 ± 0.35
PC/0.5 phr PTPP-MMT (solution)	55.6 ± 2.8	1265 ± 65	6.82 ± 0.28
PC/1 phr PTPP-MMT (solution)	59.2 ± 2.4	1378 ± 87	5.81 ± 0.22

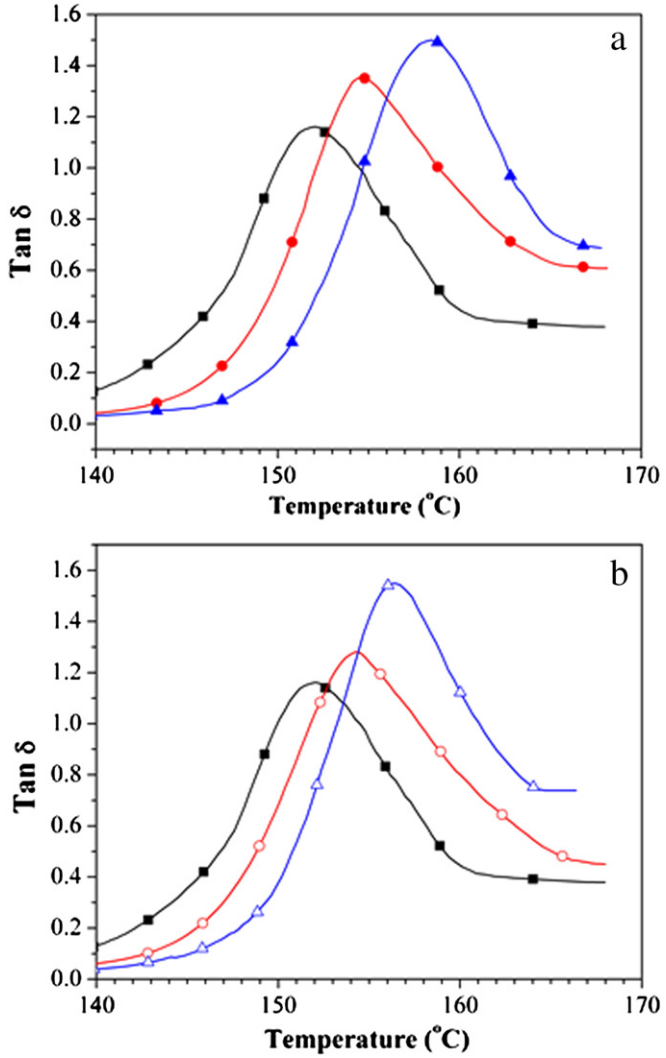

Fig. 9. Tan delta vs. temperature plots of neat PC (■); and its (a) melt blended (●,▲), (b) solution blended (○,△) nanocomposites with 0.5 phr PTPP-Mt (●,○), 1 phr PTPP-Mt (▲,△).

(1–2%) in percent transmittance occurred on incorporating PTPP-Mt into the PC matrix in both the blending techniques. The percent transmittance of pure PC (≈96% at 700 nm) was decreased to ≈95% and ≈94% on incorporating 0.5 and 1phr PTPP-Mt into the PC matrix in both the melt and solution processed nanocomposites. As the percent transmittance of the pure PC and the PC/PTPP-Mt nanocomposites fall into a very narrow region (96–94%), and independent of the techniques for nanocomposites preparation, the effect of the degradation of PTPP-Mt can be ruled out and reflection or refraction of some fraction of incident light by the clay mineral layers may be assumed to be responsible for the slight decrease in the nanocomposites.

5. Conclusions

Optically transparent PC/PTPP-Mt nanocomposites with enhanced mechanical property have successfully been prepared by both melt and solution blending techniques. Irrespective of clay mineral loadings, a highly exfoliated morphology of the clay mineral layers in the nanocomposites was evident from the XRD analysis. However, the TEM microstructures revealed the presence of some localized zones of clay at higher loading of PTPP-Mt. Negligible increment in T_g was evident from both the DSC and DMA analysis. The PC/PTPP-Mt nanocomposites possessed greater thermal stability compared to the pure PC and were

Table 2
The variation in thermal, as well as, mechanical properties in different polymer/clay mineral nanocomposites systems.

Research group	Polymer used	Clay used	T_g	Thermal stability	Tensile strength	Young modulus	Elongation at break
Cai et al.	ABS	Hexadecyl triphenyl phosphonium modified Mt	-	0.7 °C increase	-	-	-
Cetyl pyridium modified Mt	-	9.8 °C increase	-	-	-		
Sain et al.	PS	Na-Mt	30 °C increase	17 °C increase	-	-	-
Cloisite-20A	15 °C increase	8 °C increase	-	-	-		
Su et al.	PS	N-methyl-N, N-di(vinylbenzyl) octadecayl ammonium modified Mt (5 wt%)	-	Higher than pure PS	7.66 MPa decrease	0.07 GPa decrease	0.5 % increase
PMMA	-	Higher than pure PMMA	12.39 MPa increase	0.5 GPa increase	0.7 % decrease		
Xie et al.	PMMA	Na-Mt	11 °C increase	5 °C increase	-	-	-
Yeh et al.	PMMA	Dimethyl dihexadecyl ammonium modified Mt	22 °C increase	14.9 °C increase	-	-	-
Alkylphosphonium modified Mt	16 °C increase	15.9 °C increase	-	-	-		
Hasegawa et al.	PS	Octadecyl trimethylammonium modified Mt	2 °C increase	-	~ 6 MPa increase	~ 0.4 MPa decrease	~ 2% increase
Hsieh et al.	PC	Cloisite 25A (5 wt%)	9.3 °C decrease	decreases	~ 8 MPa increase	-	-
Sinha Ray et al.	PC	Synthetic fluorohectorite (SFH)	No change	-	4 MPa increase	0.3 GPa increase	-
dimethyldioctadecylammonium cation modified SFH (5 wt%)	13 °C decrease	-	25 MPa increase	2 GPa increase	-		
Nevalainen et al.	PC	Nanomer I.30P (5 wt%)	9 °C decrease	23 °C increase	(5–12) % increse	18% increase	90 % decrease
Nanomer I.34TCN (5 wt%)	10 °C decrease	18 °C increase	(0.5–6) % increase	30% increase	90 % decrease		
Carrion et al.	PC	Bentone 2010	17 °C decrease	26 °C increase	-	-	-

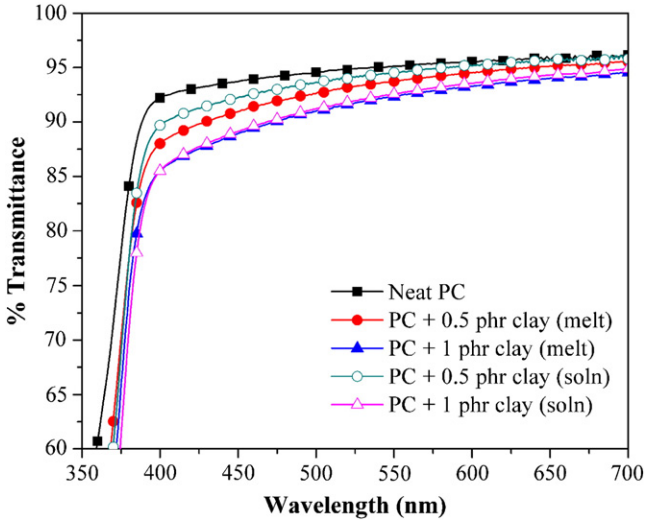

Fig. 10. UV–vis plots of Neat PC and PC/PTPP-Mt nanocomposites.

dependent on the loadings of PTPP-Mt. The tensile strength and Young modulus of PC were increased, whereas, the percent elongation was decreased with increase in the amount of PTPP-Mt in the PC/PTPP-Mt nanocomposites. The retention of optical transparency of the PC in the PC/PTPP-Mt nanocomposites with concomitant increase in mechanical properties may broaden the area of its application with an improved performance.

Acknowledgements

S. Suin is grateful to Council of Scientific and Industrial Research (CSIR), New Delhi, India, for their kind financial assistance.

References

Avalos, F., Ortiz, J.C., Zitzumbo, R., López-Manchado, M.A., Verdejo, R., Arroyo, M., 2009. Phosphonium salt intercalated montmorillonites. Appl. Clay Sci. 43, 27–32.
Bailey, S.W., 1980. Crystal structure of clay minerals and their x-ray identification. Mineralogical Society, London.
Bailey, S.W., 1984. Reviews in mineralogy. Mineralogical Society of America, Blacksburg.
Cai, Y., Huang, F., Xia, X., Wei, Q., Tong, X., Wei, A., Gao, W., 2010. Comparison between structures and properties of ABS nanocomposites derived from two different kinds of OMT. J. Mater. Eng. Perform. 19, 171–176.
Calderon, J.U., Lennox, B., Kamal, M.R., 2008. Thermally stable phosphonium-montmorillonite organoclays. Appl. Clay Sci. 40, 90–98.
Carrion, F.J., Arribas, A., Bermudez, M.D., Guillamon, A., 2008. Physical and tribological properties of a new polycarbonate-organoclay nanocomposite. Eur. Polym. J. 44, 968–977.
Chow, W.S., Neoh, S.S., 2010. Mechanical, morphological and thermal properties of polycarbonate/SEBS-g-MA/montmorillonite nanocomposites. Polym. Plast. Technol. Eng. 49, 62–68.
Cui, L., Bara, J.E., Brun, Y., Yoo, Y., Yoon, P.J., Paul, D.R., 2009. Polyamide- and polycarbonate-based nanocomposites prepared from thermally stable imidazolium organoclay. Polymer 50, 2492–2502.
Feng, J., Hao, J., Du, J., Yang, R., 2012. Using TGA/FTIR TGA/MS and cone calorimetry to understand thermal degradation and flame retardancy mechanism of polycarbonate filled with solid bisphenol A bis(diphenyl phosphate) and montmorillonite. Polym. Degrad. Stab. 97, 605–614.
Friessell, W.J., Bikales, N.M., 1967. Encyclopedia of polymer science and technology, vol. 6. John Wiley and Sons Inc., New York pp. 740–755.
Gao, Z., Xie, W., Hwu, J.M., Wells, L., Pan, W.P., 2001. The characterization of organic modified montmorillonite and its filled PMMA nanocomposite. J. Therm. Anal. Calorim. 64, 467–475.
Gilman, J.W., Awad, W.H., Davis, R.D., Shields, J., Harris Jr., R.H., Davis, C., Morgan, A.B., Sutto, T.E., Callahan, J., Trulove, P.C., DeLongr, H.C., 2002. Polymer/layered silicate nanocomposites from thermally stable trialkylimidazolium-treated montmorillonite. Chem. Mater. 14, 3776–3785.
Guduri, B.R., Luyt, A.S., 2008. Structure and mechanical properties of polycarbonate modified clay nanocomposites. J. Nanosci. Nanotechnol. 8, 1880–1885.
Hasegawa, N., Okamoto, H., Kawasumi, M., Usuki, A., 1999. Preparation and mechanical properties of polystyrene-clay hybrids. J. Appl. Polym. Sci. 74, 3359–3364.
Hsieh, A.J., Moy, P., Beyer, F.L., Madison, P., Napadensky, E., Ren, J., Krishnamoorti, R., 2004. Mechanical response and rheological properties of polycarbonate layered-silicate nanocomposites. Polym. Eng. Sci. 44, 825–837.
Huang, X., Lewis, S., Brittain, W.J., Vaia, R., 2000. Synthesis of polycarbonate-layered silicate nanocomposites via cyclic oligomers. Macromolecules 33, 2000–2004.
Jash, P., Wilkie, C.A., 2005. Effects of surfactants on the thermal and fire properties of poly(methyl methacrylate)/clay nanocomposites. Polym. Degrad. Stab. 88, 401–406.
Lagaly, G., Beneke, K., 1991. Intercalation and exchange reactions of clay minerals and non-clay layer compounds. Colloid Polym. Sci. 269, 1198–1211.
Lee, K.M., Han, C.D., 2003. Effect of hydrogen bonding on the rheology of polycarbonate/organoclay nanocomposites. Polymer 44, 4573–4588.
LeGrand, D.G., Bendler, J.T., 2000. Mechanical properties of polycarbonates. Handbook of polycarbonate science and technologyMarcel Dekker, Inc., New York pp. 107–125.
Lu, C., Mai, Y.W., 2005. Influence of aspect ratio on barrier properties of polymer-clay nanocomposites. Phys. Rev. Lett. 95 (088303(1)-088303(4)).
Lu, H., Nutt, S., 2003. Restricted relaxation in polymer nanocomposites near the glass transition. Macromolecules 36, 4010–4016.
Mishra, J.K., Hwang, K.H., Ha, C.S., 2005. Preparation, mechanical and rheological properties of a thermoplastic polyolefin (TPO)/organoclay nanocomposite with reference to the effect of maleic anhydride modified polypropylene as a compatibilizer. Polymer 46, 1995–2002.
Mitsunaga, M., Ito, Y., Sinha, Ray S., Okamoto, M., Hironaka, K., 2003. Intercalated polycarbonate/clay nanocomposites: Nanostructure control and foam processing. Macromol. Mater. Eng. 288, 543–548.
Nevalainen, K., Vuorinen, J., Villman, V., Suihkonen, R., Jarvela, P., Sundelin, J., Lepisto, T., 2009. Characterization of twin-screw-extruder-compounded polycarbonate nanoclay composites. Polym. Eng. Sci. 9, 630–640.
Patro, T.U., Khakhar, D.V., Misra, A., 2009. Phosphonium-based layered silicate-poly(ethylene terephthalate) nanocomposites: Stability, thermal and mechanical properties. J. Appl. Polym. Sci. 113, 1720–1732.
Rama, M.S., Swaminathan, S., 2010. Polycarbonate/clay nanocomposites via in situ melt polycondensation. Ind. Eng. Chem. Res. 49, 2217–2227.
Sain, S., Khatua, B.B., 2011. Synthesis of highly exfoliated PS/Na^+-MMT nanocomposites by suspension polymerization using Na^+-MMT clay platelets as suspension stabilizer. Macromol. Res. 19, 44–52.
Saitoh, K., Ohashi, K., Oyama, T., Takahashi, A., Kadota, J., Hirano, H., Hasegawa, K., 2011. Development of high-performance epoxy/clay nanocomposites by incorporating novel phosphonium modified montmorillonite. J. Appl. Polym. Sci. 122, 666–675.
Sinha Ray, S., Okamoto, M., 2003. Polymer/layered silicate nanocomposites: A review from preparation to processing. Prog. Polym. Sci. 28, 1539–1641.
Su, S., Wilkie, C.A., 2003. Exfoliated poly(methyl methacrylate) and polystyrene nanocomposites occur when the clay cation contains a vinyl monomer. J. Polym. Sci. A Polym. Chem. 41, 1124–1135.
Suin, S., Khatua, B.B., 2012. Exfoliated and optically transparent polycarbonate/clay nanocomposites using phosphonium modofied organoclay: preparation and characterizations. Ind. Eng. Chem. Res. 51, 15096–15108.
Suin, S., Shrivastava, N.K., Maiti, S., Khatua, B.B., 2013. Phosphonium modified organoclay as potential nanofiller for the development of exfoliated and optically transparent polycarbonate/clay nanocomposites: Preparation and characterizations. Eur. Polym. J. 49, 49–60.
Theng, B.K.G., 1974. The chemistry of clay organic reactions. Adam Hilger, London.
Wang, W.S., Liang, C.K., Chen, Y.C., Su, Y.L., Tsai, T.Y., Chen-Yang, Y.W., 2012. Transparent and flame retardant PMMA/clay nanocomposites prepared with dual modified organoclay. Polym. Adv. Technol. 23, 625–631.
Wu, D., Wu, L., Zhang, M., Wu, L., 2007. Effect of epoxy resin on rheology of polycarbonate/clay nanocomposites. Eur. Polym. J. 43, 1635–1644.
Xiang, C., Zao, T.S., Hua, L.M., Ting, W., Fu, L.R., Biao, Y.U., 2010. Thermal stability and long-acting antibacterial activity of phosphonium montmorillonites. J. Cent. S. Univ. Technol. 17, 485–491.
Xie, W., Gao, Z., Pan, W.P., Hunter, D., Singh, A., Vaia, R., 2001. Thermal degradation chemistry of alkyl quaternary ammonium montmorillonite. Chem. Mater. 13, 2979–2990.
Xie, W., Xie, R., Pan, W.P., Hunter, D., Koene, B., Tan, L.S., Vaia, R., 2002. Thermal stability of quaternary phosphonium modified montmorillonites. Chem. Mater. 14, 4837–4845.
Xie, T., Yang, G., Fang, X., Ou, Y., 2003. Synthesis and characterization of poly(methyl methacrylate)/montmorillonite nanocomposites by in situ bulk polymerization. J. Appl. Polym. Sci. 89, 2256–2260.
Yeh, J., Liou, S., Lai, M., Chang, Y., Huang, C., Chen, C.P., Jaw, J.H., Tsai, T.Y., Yu, Y.H., 2004. Comparative studies of the properties of poly(methyl methacrylate)/clay nanocomposite materials prepared by in situ emulsion polymerization and solution dispersion. J. Appl. Polym. Sci. 94, 1936–1946.
Yoon, P.J., Hunter, D.L., Paul, D.R., 2003a. Polycarbonate nanocomposites. Part 1. Effect of organoclay structure on morphology and properties. Polymer 44, 5323–5339.
Yoon, P.J., Hunter, D.L., Paul, D.R., 2003b. Polycarbonate nanocomposites: Part 2. Degradation and color formation. Polymer 44, 5341–5354.
Yu, Y.H., Lin, C.Y., Yeh, J.M., Lin, W.H., 2003. Preparation and properties of poly(vinyl alcohol)-clay nanocomposite materials. Polymer 44, 3553–3560.
Zheng, X., Wilkie, C.A., 2003. Flame retardancy of polystyrene nanocomposites based on an oligomeric organically-modified clay containing phosphate. Polym. Degrad. Stab. 81, 539–550.